Journal of Solid State Chemistry 183 (2010) 1437–1441

Contents lists available at ScienceDirect

Journal of Solid State Chemistry

journal homepage: www.elsevier.com/locate/jssc

Preparation and photoluminescence properties of *RE*:$Na_3La_9O_3(BO_3)_8$ (*RE*=Er, Yb) crystals

Zuoliang Liu [a,b], Guochun Zhang [a,*], Jianxiu Zhang [a], Xiaoyan Bai [a,b], Peizhen Fu [a], Yicheng Wu [a]

[a] Key Laboratory of Functional Crystals and Laser Technology, Technical Institute of Physics and Chemistry, Chinese Academy of Sciences, Beijing 100190, China
[b] Graduate School of the Chinese Academy of Sciences, Beijing 100039, China

ARTICLE INFO

Article history:
Received 31 October 2009
Received in revised form
12 April 2010
Accepted 14 April 2010
Available online 21 April 2010

Keywords:
RE:$Na_3La_9O_3(BO_3)_8$ (*RE*=Er, Yb)
Photoluminescence properties
Top seed solution growth (TSSG)
Self-frequency doubling (SFD)

ABSTRACT

Using Na_2CO_3–H_3BO_3–NaF as fluxes, transparent *RE*:$Na_3La_9O_3(BO_3)_8$ (abbr. *RE*:NLBO, *RE*=Er, Yb) crystals have been grown by the top seed solution growth (TSSG) method. The X-ray powder diffraction analysis shows that the *RE*:NLBO crystals have the same structure with NLBO. The element contents were determined by molar to be 0.64% Er^{3+} in Er:NLBO, 2.70% Yb^{3+} in Yb:NLBO, respectively. The polarized absorption spectra of *RE*:NLBO have been measured at room temperature and show that both Er:NLBO and Yb:NLBO have a strong absorption bands near 980 nm with wide FWHM (Full Wave at Half Maximum) (21 nm for Er:NLBO and 25 nm for Yb:NLBO). Fluorescence spectra have been recorded. Yb:NLBO has the emission peaks at 985 nm, 1028 nm and 1079 nm and the emission peak of Er:NLBO is at 1536 nm. Spectral parameters have been calculated by the Judd–Ofelt theory for Er:NLBO and the reciprocity method for Yb:NLBO, respectively. The calculated values show that Er:NLBO is a candidate of 1.55 μm laser crystals and Yb:NLBO is a candidate for self-frequency doubling crystal.

1. Introduction

Self-frequency doubling (SFD) crystals, which have both active ions to produce laser and nonlinear properties to transfer the light frequency, have been of great interest because of their advantage of low cost and high compactness. Some rare earth doped borates have been found to be SFD crystals, such as Nd:$YAl_3(BO_3)_4$ (NYAB) [1], Yb:$YAl_3(BO_3)_4$ (YbYAB) [2], Nd:$YCa_4O(BO_3)_3$ (Nd:YCOB) [3], Yb:$YCa_4O(BO_3)_3$ (Yb:YCOB) [4], Nd:$Ca_4GdO(BO_3)_3$ (Nd:GdCOB) [5] and Nd:$La_2CaB_{10}O_{19}$ (Nd:LCB) [6].

$Na_3La_9O_3(BO_3)_8$ (NLBO) crystal, discovered in 2002 [7], has been investigated as a potential nonlinear crystal with strong SHG effect [8]. Theoretical simulations of linear and nonlinear optical susceptibilities of $Na_3La_9O_3(BO_3)_8$ were reported in 2008 [9]. The calculated values are in good agreement with the experimental data and show that NLBO crystalline may present matrix a great potential due to large values of the dispersion of the second order susceptibilities. In NLBO crystal, La^{3+} ions could be partially or completely substituted by active ions such as Nd^{3+}, Er^{3+} and Yb^{3+}, etc to produce laser. Recently, more attention has been focused on rare earth ion-doped NLBO and it fluorescence properties. In 2007, spectral properties of Nd:NLBO were studied [10,11], and the result shows that Nd:NLBO is a potential SFD crystal. Time-resolved line-narrowed fluorescence spectroscopy of Eu:NLBO has been investigated [12], and four independent crystal field sites for Eu^{3+} ion in NLBO have been found.

Besides Nd^{3+} and Eu^{3+} ions, Er^{3+} and Yb^{3+} are usually used as active ions. Er^{3+}doped materials are widely studied due to the application of 1.55 μm laser for eye-safe, in optical communication and laser radar, etc. Yb^{3+} ion has only two manifolds, the ground state $^2F_{7/2}$ and the excited state $^2F_{5/2}$, simpler than Nd^{3+} ion. Yb^{3+} doped crystals have the advantages of no luminescence quenching, no upconversion and excited-state absorption. Some Yb^{3+} doped crystals, such as Yb:YAB, Yb:GdCOB and Yb:LCB, have been investigated as SFD crystals. Moreover, Yb^{3+} ions in the borate matrices cause some crucial nonlinear optical effects, like photoinduced changes of the second harmonic generation [13,14]. In this paper, we report the growth of Er^{3+} and Yb^{3+}-doped NLBO crystals and their photoluminescence properties.

2. Experimental procedures

2.1. Synthesis and growth

Since NLBO melts incongruently, *RE*:NLBO has been grown using Na_2CO_3–H_3BO_3–NaF as fluxes by the top seed solution method (TSSG) [15]. Analytical grade H_3BO_3, Na_2CO_3, 99.99% purity La_2O_3, Er_2O_3 and Yb_2O_3 were used as starting materials. The polycrystalline samples of Er:NLBO and Yb:NLBO were synthesized by the solid-state reaction technique in stoichiometric proportions of $Na_3(Er_{0.02}La_{0.98})_9O_3(BO_3)_8$ and $Na_3(Yb_{0.1}La_{0.9})_9O_3(BO_3)_8$, respectively. Then the solvent

* Corresponding author. Fax: +86 10 82543726.
E-mail address: gczhang@mail.ipc.ac.cn (G. Zhang).

0022-4596/$ - see front matter © 2010 Elsevier Inc. All rights reserved.
doi:10.1016/j.jssc.2010.04.026

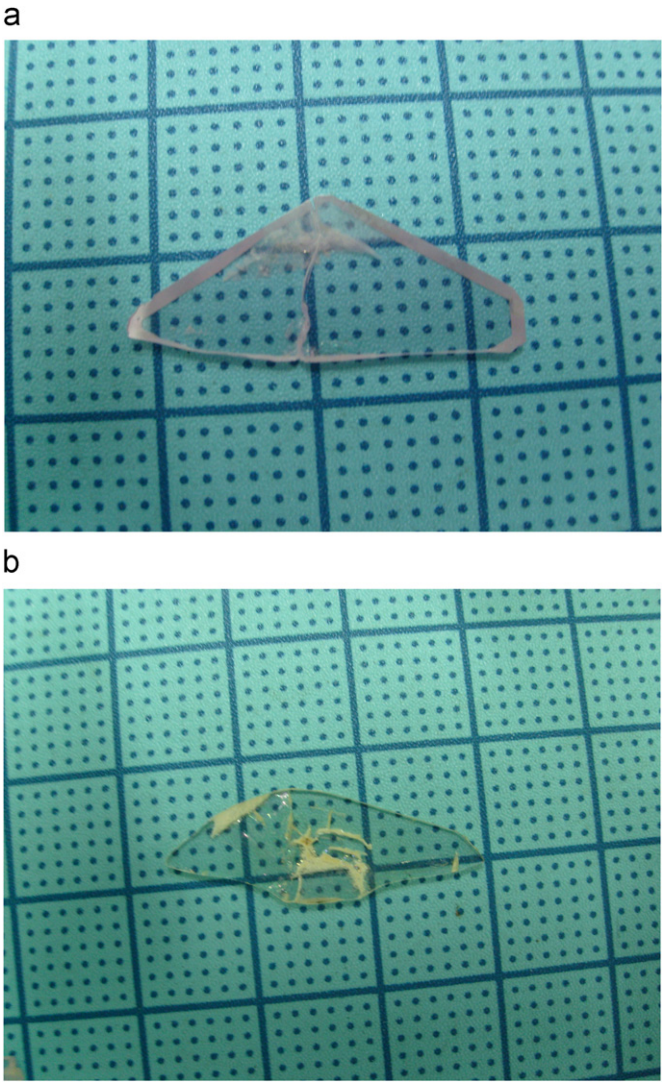

Fig. 1. Photograph of polished crystals (a) Er:NLBO and (b) Yb:NLBO.

Na_2CO_3–H_3BO_3–NaF was added into the above synthesized polycrystalline samples in proportion of *RE*:NLBO:Na_2CO_3:H_3BO_3:NaF= 1.0:6.0:6.0:7.5 (molar ratio). After ground, the mixture was melted into a Pt crucible (60 mm diameter and 60 mm height) and held at 1100 °C for 24 h. The saturation temperature was determined using a testing seed crystal to be about 973 °C for Er:NLBO and 970 °C for Yb:NLBO, respectively. The seed crystal with [1 0 0] direction was slowly introduced into the furnace and dipped into the solution at a temperature 10 °C above the saturation temperature to avoid crack. Afterwards, the temperature was lowered to the saturation temperature within 30 min. The cooling rate was 0.2–0.4 °C/day and the rotating rate was 10–20 rpm. Ten days later, the crystal was drawn out of the melt and cooled down to room temperature at a rate of 5 °C/h. Partially transparent pink Er:NLBO and colorless Yb:NLBO crystals were obtained, respectively. After sliced and polished, the transparent Er:NLBO and Yb:NLBO crystal pieces are shown in Fig. 1.

2.2. Properties measurements

X-ray powder diffraction analyses were performed on a BRUKER D8 ADVANCE X-ray powder diffractometer with Cu$K\alpha$ radiation (graphite monochromator). The scanning step width of 0.03° and the scanning rate of 0.03° s^{-1} were applied to record the patterns in the 2θ range of 7°–70°. Component analyses in the crystal were carried out on a Thermo ICP-MS XII inductively coupled plasma mass spectrometry (ICP-MS). The polarized absorption spectra of polished Er:NLBO and Yb:NLBO crystals were recorded with a Lambda-900 UV–VIS–NIR spectrophotometer with the spectral resolution of 8 nm at room temperature. FL3-12 fluorescence spectrometer with the spectral resolution of 0.2 nm (Xe lamp as light source) was used to measure fluorescence spectra at room temperature.

3. Results and discussion

3.1. X-ray powder diffraction

Fig. 2 shows the X-ray powder diffraction patterns of the Er:NLBO and Yb:NLBO crystals. All peaks in the powdered patterns of Er:NLBO and Yb:NLBO crystals could be indexed on the basis of the hexagonal system using the TREOR 90 program [16], which are in good agreement with that of NLBO crystal. It indicates that the substitution of Er^{3+} or Yb^{3+} ions for La^{3+} ion did not cause the variation of crystal structure.

3.2. Er^{3+} and Yb^{3+} content determination

Er:NLBO and Yb:NLBO crystals were weighed, ground into powder, dissolved into dilute nitric acid for analysis. The element contents were determined by molar to be 0.64% Er^{3+} in Er:NLBO, 2.70% Yb^{3+} in Yb:NLBO, respectively. The segregation coefficients were 0.32 for Er^{3+} and 0.27 for Yb^{3+}, respectively. In contrast with the segregation coefficient (1.05) [10] of Nd^{3+}(110.9 pm, coordination no.=8) in Nd:NLBO, the less segregation coefficients of Er^{3+} and Yb^{3+} result from the large difference between the radii of Er^{3+}(100.4 pm, coordination no.=8) and Yb^{3+}(98.5 pm, coordination no.=8) with La^{3+}(116.0 pm, coordination no.=8) [17].

3.3. Absorption spectra

Er:NLBO has absorption bands at 366, 379, 407, 452, 488, 524, 543, 651, 804, 982 and 1536 nm corresponding to the transition of Er^{3+} from ground state $^4I_{15/2}$ to excited states $^4G_{9/2}$, $^4G_{11/2}$, $^2H_{9/2}$, $^4F_{5/2}$, $^4F_{7/2}$, $^2H_{11/2}$, $^4S_{3/2}$, $^4F_{9/2}$,$^4I_{9/2}$, $^4I_{11/2}$ and $^4I_{13/2}$, respectively, while Yb:NLBO only has one absorption band at 983 nm

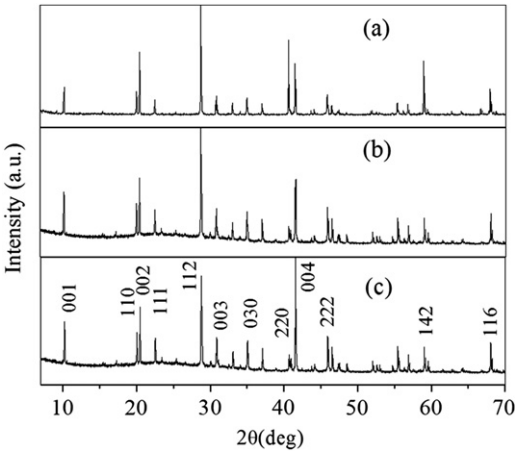

Fig. 2. XRD Powder patterns of (a) NLBO, (b) Er:NLBO and (c) Yb:NLBO.

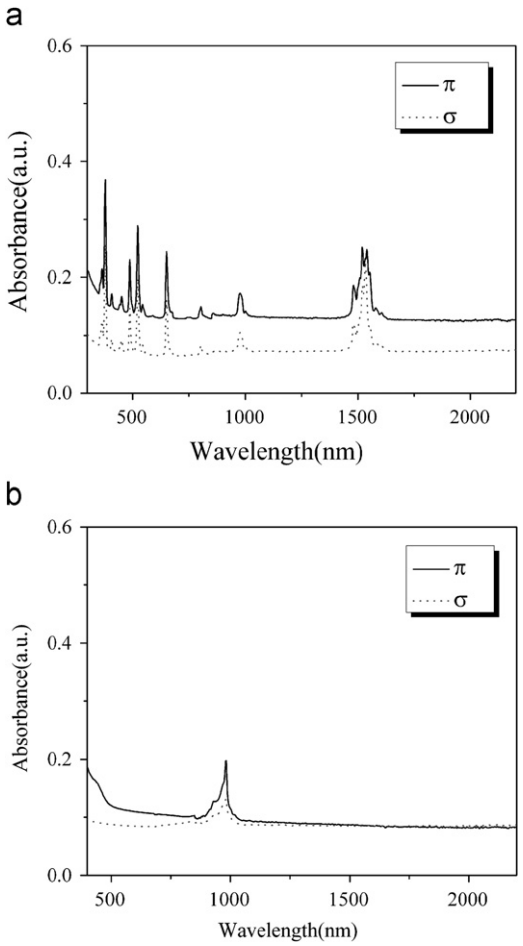

Fig. 3. Polarized absorption spectra of (a) Er:NLBO and (b) Yb:NLBO, the solid lines are π-polarization and the dotted lines are σ-polarization.

corresponding to $^2F_{7/2}\rightarrow{}^2F_{5/2}$ transition, as shown in Fig. 3. Absorptions at 982 nm of Er^{3+} ion, 983 nm of Yb^{3+} ion were paid more attention because they could be pumped by InGaAs diode laser. Their absorption cross-sections were calculated to be $\sigma_{abs-982}=0.33\times10^{-20}\,cm^2$ of σ-polarization and $0.56\times10^{-20}\,cm^2$ of π-polarization for Er^{3+} in Er:NLBO; $\sigma_{abs-983}=0.74\times10^{-20}\,cm^2$ of σ-polarization and $1.23\times10^{-20}\,cm^2$ of π-polarization for Yb^{3+} in Yb:NLBO, respectively. Both the crystals have larger absorption of π-polarization than that of σ-polarization. The FWHM of Er:NLBO crystal at 982 nm was 21 nm and the FWHM of Yb:NLBO crystal at 983 nm was 25 nm. Both of them could be suitably pumped by InGaAs laser diode without exactly controlling the temperature.

3.4. Fluorescence spectra

Fig. 4 shows the fluorescence spectra of the Yb:NLBO at the range of 900–1200 nm and Er:NLBO at the range of 1400–1700 nm. Yb:NLBO had three emission bands with the peaks at 985, 1028 and 1079 nm corresponding to the Stark electronic levels. Peak of the main emission band of Er:NLBO was at 1536 nm, corresponding to the transition of $^4I_{15/2}\rightarrow{}^4I_{13/2}$. The fluorescence lifetimes were obtained using a single-exponential decay fit to be 2.33 ms for Er:NLBO at 1536 nm and 1.05 ms for Yb:NLBO at 1028 nm, respectively. Fitting curves are shown in Fig. 5.

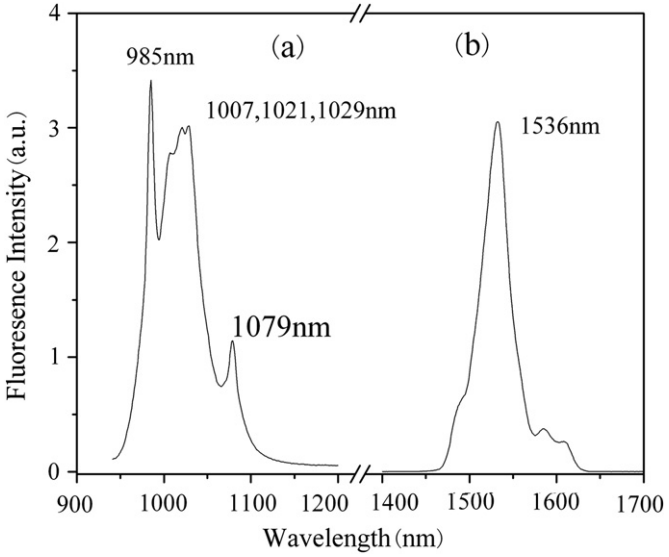

Fig. 4. Fluorescence spectra of (a) Yb:NLBO and (b) Er:NLBO.

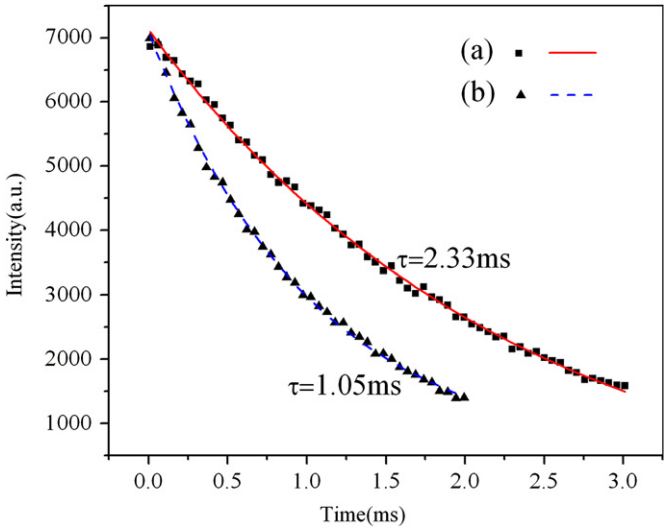

Fig. 5. Fluorescence lifetimes of (a) Er:NLBO (at 1536 nm) and (b) Yb:NLBO (at 1028 nm).

3.5. Spectral parameters

3.5.1. Er:NLBO

The spectral parameters of f–f transitions for Er^{3+} in Er:NLBO crystal are characterized by the Judd–Ofelt (JO) theory [18,19]. The experimental absorption line strengths S_{exp} from the ground state J to the excited state J' are related to the integrated absorption coefficient $\int K(\lambda)d\lambda$.

$$S_{exp}(J\rightarrow J')=\frac{3ch(2J+1)}{8\pi^3N_0\bar{\lambda}e^2}\frac{9n}{(n^2+2)^2}\int K(\lambda)d\lambda, \quad (1)$$

where c is the velocity of light, e the electron charge, m the electron mass, h the Planck's constant, N_0 the Er^{3+} ions density, $\bar{\lambda}$ the mean wavelength of the absorption band, n the mean refractive index of the crystal at the mean wavelength $\bar{\lambda}$ and J and J' the total angular-momentum quantum number of the initial and final states, respectively. $\int K(\lambda)d\lambda$ can be calculated by the following expression:

$$\int K(\lambda)d\lambda=\frac{2.3}{L}\int D(\lambda)d\lambda, \quad (2)$$

where L is the thickness of the sample and $D(\lambda)$ the absorbance (optical density).

Because the magnetic dipole line strength for $^4I_{15/2}\rightarrow{}^4I_{13/2}$ transition exerts a considerable effect on total radiative probabilities, it cannot be neglected. The magnetic dipole line strength can be obtained using the following equation [20]:

$$F_{md}=\frac{8\pi^2 mc}{3h(2J+1)\bar{\lambda}}S_{md} \tag{3}$$

where F_{md} is the oscillator strength calculated by Carnall et al. [21].

Then the electric dipole line strength can be obtained by subtracting S_{md} from S_{exp}

$$S_{ed}=S_{exp}-S_{md} \tag{4}$$

According to the JO theory, the calculated absorption line strengths S_{ed} can also be expressed in terms of JO parameter $\Omega_{2,4,6}$ as

$$S_{ed}(J\rightarrow J')=\sum_{t=2,4,6}\Omega_t|\langle \Phi J\|U^{(t)}\|\Phi' J'\rangle|^2, \tag{5}$$

The reduced tensor matrix elements $|\langle \Phi J\|U^{(t)}\|\Phi' J'\rangle|^2$ are almost independent of the host environment and the values of the matrix elements are taken from Weber [22]. A least-squares fitting provides the values of the three JO parameters: $\Omega=1.99\times10^{-20}\,cm^2$, $\Omega_4=1.10\times10^{-20}\,cm^2$ and $\Omega_6=1.72\times10^{-20}\,cm^2$ for σ-polarization and $\Omega_2=1.39\times10^{-20}\,cm^2$, $\Omega_4=0.55\times10^{-20}\,cm^2$ and $\Omega_6=1.33\times10^{-20}\,cm^2$ for π-polarization, respectively. The root mean square deviation rms-ΔS between the experimental and calculated line strengths is $0.18\times10^{-20}\,cm^2$ and $0.13\times10^{-20}\,cm^2$.

Using the determined JO parameters, the line strengths for the transitions from an excited level to the lower manifolds can be calculated. And the radiative transition rate $A(J\rightarrow J')$ for the transitions can be calculated from the following equation:

$$A(J\rightarrow J')=\frac{64\pi^4 e^2}{3h(2J+1)\bar{\lambda}^3}\left[\frac{n(n^2+2)^2}{9}S_{ed}+n^3S_{md}\right], \tag{6}$$

Then the radiative lifetime τ_{rad} and the branching ratio $\beta_{J\rightarrow J'}$ can be obtained by

$$\tau_{rad}=1/\sum_{J'}A(J\rightarrow J'), \tag{7}$$

$$\beta_{J\rightarrow J'}=A(J\rightarrow J')/\sum_{J'}A(J\rightarrow J'). \tag{8}$$

The results are listed in Table 1.

The integrated emission cross-section Σ can be calculated as

$$\sum(J\rightarrow J')=(\lambda^2/8\pi cn^2)A(J\rightarrow J'). \tag{9}$$

To make a further evaluation, a comparison between Er:NLBO and other Er^{3+} doped crystals of $^4I_{13/2}\rightarrow{}^4I_{15/2}$ transition parameters is listed in Table 2. In terms of Caird's point [23], Er:NLBO has the largest integrated emission cross-section Σ so that Er:NLBO probably produces laser emission about 1.55 μm. The radioactive transition rate A of Er:NLBO equals to the value of Er:YAB, but larger than the value of Er:YAG, which has demonstrated to produce 1.55 μm laser. Thus, Er:NLBO is probably used to produce 1.55 μm laser. In addition, due to the great SHG coefficient of NLBO, Er:NLBO is recognized as a potential SFD crystal.

3.5.2. Yb:NLBO

Although Yb:NLBO has three emission bands, only 1028 nm and 1079 nm may be used to yield laser owing to the overlap between emission band and absorption band of 985 nm. The emission band of 1028 nm is stronger, so we have calculated the laser parameters at 1028 nm.

Table 1
The spectral parameters for Er^{3+} in Er:NLBO crystal.

Transitions		$\bar{\lambda}$ (nm)	σ-polarization		π-polarization		τ_r (μs)
			A (s^{-1})	β_c	A(s^{-1})	β_c	
$^4I_{13/2}\rightarrow$	$^4I_{15/2}$	1520	205.64 56.52	1	159.60 56.52	1	4221
$^4I_{11/2}\rightarrow$	$^4I_{13/2}$	2727	29.97	0.1366	22.61	0.125	4266
	$^4I_{15/2}$	976	260.59	0.8634	157.73	0.875	
$^4F_{9/2}\rightarrow$	$^4I_{9/2}$	3613	1.73	0.001	1.34	0.001	599
	$^4I_{11/2}$	2010	106.40	0.05	81.69	0.0584	
	$^4I_{13/2}$	1157	82.54	0.04	52.05	0.0372	
	$^4I_{15/2}$	657	1873.64	0.91	1264.7	0.9035	
$^4S_{3/2}\rightarrow$	$^4I_{9/2}$	1705	46.05	0.01	32.14	0.0139	369
	$^4I_{11/2}$	1239	68.66	0.02	52.51	0.0228	
	$^4I_{13/2}$	852	904.75	0.28	699.60	0.3034	
	$^4I_{15/2}$	546	2255.47	0.69	1521.55	0.6599	
$^2H_{9/2}\rightarrow$	$^4F_{9/2}$	1055	49.13	0.01	32.70	0.0116	280
	$^4I_{9/2}$	817	17.43	0.004	11.67	0.0041	
	$^4I_{11/2}$	692	495.03	0.10	332.62	0.1184	
	$^4I_{13/2}$	552	2181.61	0.45	1582.73	0.5632	
	$^4I_{15/2}$	405	2126.22	0.44	850.49	0.3026	

Table 2
Comparison of spectral parameters of $^4I_{13/2}\rightarrow{}^4I_{15/2}$ transition of Er doped crystals.

Crystals	Transitions	λ (nm)	A (s^{-1})	∑ (10^{-18} cm)
Er:NLBO σ	$^4I_{13/2}\rightarrow{}^4I_{15/2}$	1520	262	2.87
π			216	2.37
Er:YAG [24]			211	2.00
Er:YAB [25]			262.9	2.58

The JO theory can be performed only on the ions with more than two manifolds. Due to two manifolds of Yb ($^2F_{7/2}$ and $^2F_{5/2}$), the parameters of Yb:NLBO are calculated using the reciprocity method (RM) [26] here. The emission cross-section can be obtained by the reciprocity method using the following formula:

$$\sigma_{em}(\nu)=\sigma_{abs}(\nu)\frac{Z_l}{Z_u}\exp[(E_{zl}-h\nu)/kT] \tag{10}$$

where σ_{abs} is the absorption cross section, Z_l and Z_u the partition functions of lower and up energy levels, E_{zl} the zero level energy which can be obtained by the emission spectra, h the Planck's constant, k the Boltzmann's constant and T the absolute temperature. The partition function can be calculated using the following formula:

$$Z_k=\sum_k d_k\exp(-E_k/kT) \tag{11}$$

where d_k is the degree of degeneracy.

β_{min}, which is defined as the minimum fraction of Yb^{3+} ions that must be excited to balance the gain exactly with the ground state absorption at λ_{ext}, can be obtained from the following formula:

$$\beta_{min}=\frac{\sigma_{abs}(\lambda_{ext})}{\sigma_{em}(\lambda_{ext})+\sigma_{abs}(\lambda_{ext})} \tag{12}$$

By combining Eqs. (1) and (2), β_{min} also can be expressed as follows:

$$\beta_{min}=\{1+(Z_l/Z_u)\exp[(E_{zl}-h\nu)/kT]\}^{-1} \tag{13}$$

Table 3
Spectral parameters of Yb doped crystals.

Crystal	Yb:NLBO		Yb:LCB [27]	Yb:YAB [28]	Yb:YCOB [29]	Yb:GdCOB [30]	Yb:YAG [31]
λ_p (nm)	983		976	975	976	902	942
λ_{ext} (nm)	1028		1031	1040	1030	1032	1031
σ_{abs} (10^{-20} cm^2)	0.74^{σ}	1.23^{π}	1.16	3.4	0.94	0.41	0.8
σ_{em} (10^{-20} cm^2)	1.83		3.51	0.8	0.55	0.55	2.0
τ_{em} (ms)	1.05		0.95	0.68	2.56	2.60	1.08
I_{sat} (KW/cm^2)	27.9^{σ}	25.1^{π}	18.5	8.8	8.2	25.5	28.0
β_{min} (%)	10.5^{σ}	11.5^{π}	6.4	4.3	5.8	6.0	5.5
I_{min} (KW/cm^2)	2.93^{σ}	2.88^{π}	1.18	0.38	0.48	1.54	1.54
FWHM (nm)	25	15	20		2.6	2.6	

σ: values of σ-polarization.π: values of π-polarization.

I_{sat} is the pump saturation intensity, which can be calculated from the following formula:

$$I_{sat} = hc/(\lambda_p \sigma_{abs} \tau_{em}) \quad (14)$$

The minimum pump intensity I_{min} can be obtained from the following formula:

$$I_{min} = \beta_{min} I_{sat} \quad (15)$$

The calculated parameters of Yb:NLBO and Yb doped laser crystals are listed in Table 3.

In comparison with other Yb doped SFD crystals, Yb:NLBO has a broader FWHM, which is very suitable for diode laser pumping. From Table 3, it is also seen that the values of I_{sat}, β_{min} and I_{min} of Yb:NLBO are larger than that of Yb:LCB, Yb:YAB and Yb:YCOB, approximately equal to Yb:GdCOB. These parameters show that Yb:NLBO is a potential self-frequency doubling crystal.

4. Conclusion

Er:NLBO and Yb:NLBO crystals have been grown by the TSSG method using Na_2CO_3–H_3BO_3–NaF as fluxes. XRD powder patterns reveal that their structures are the same with NLBO. Both the Er:NLBO and Yb:NLBO crystals have wide absorption bands at near 980 nm, which could be efficiently pumped by InGaAs laser diode. For Er:NLBO, the JO parameters are $\Omega_2 = 1.99 \times 10^{-20}$ cm^2, $\Omega_4 = 1.10 \times 10^{-20}$ cm^2 and $\Omega_6 = 1.72 \times 10^{-20}$ cm^2 for σ-polarization and $\Omega_2 = 1.39 \times 10^{-20}$ cm^2, $\Omega_4 = 0.55 \times 10^{-20}$ cm^2 and $\Omega_6 = 1.33 \times 10^{-20}$ cm^2 for π-polarization, respectively. A comparison with Er:YAB and Er:YAG indicates that Er:NLBO is a candidate of 1.55 μm laser crystals. The values of I_{sat}, β_{min}, and I_{min} of Yb:NLBO are 27.9 KW/cm^2, 10.5% and 2.93 KW/cm^2, respectively. It implies that Yb:NLBO is a candidate for self-frequency doubling crystal.

Acknowledgments

This work was financially supported by the National Natural Science Foundation of China (no. 50802100) and Beijing Natural Science Foundation (no. 2102044).

References

[1] J. Bartschke, R. Knappe, K.J. Boller, R. Wallenstein, IEEE J. Quantum Electron. 33 (1997) 2295.
[2] P. Wang, P. Dekker, J.M. Dawes, J.A. Piper, Y. Liu, Wang, J. Opt. Lett. 25 (2000) 731.
[3] J.M. Eichenholz, D.A. Hammons, L. Shah, Q. Ye, R.E. Peale, M. Richardson, B.H.T. Chai, Appl. Phys. Lett. 74 (1999) 1954.
[4] D.A. Hammons, J.M. Eichenholz, Q. Ye, B.H.T. Chai, L. Shah, R.E. Richardson, M. Richardson, H. Qiu, Opt. Commun. 156 (1998) 327.
[5] F. Mougel, G. Aka, A. Kahn-harari, H. Hubert, J.M. Bentiez, D. Viven, Opt. Mater. 8 (1997) 161.
[6] A. Brenier, Y. Wu, P. Fu, R. Guo, F. Jing, Y. Zu, Appl. Phys. B—Lasers Opt. 86 (2007) 673.
[7] P. Gravereau, J.P. Chaminade, S. Pechev, V. Nikolov, D. Ivanova, P. Peshev, Solid State Sci. 4 (2002) 993.
[8] G. Zhang, Y. Wu, Y. Li, F. Chang, S. Pan, P. Fu, C. Chen, J. Cryst. Growth 275 (2005) e1997.
[9] A.H. Reshak, S. Auluck, I.V. Kityk, J. Phys.: Condens. Matter 20 (2008) 145209/1.
[10] X. Bai, G. Zhang, P. Fu, Y. Wu, J. Chin. Rare Earth Soc. 25 (2007) 487.
[11] R. Balda, V. Jubera, C. Frayret, S. Pechev, R. Olazcuaga, P. Gravereau, J.P. Chaminade, M. Al-Saleh, Fernández, J. Opt. Mater. 30 (2007) 122.
[12] C. Cascales, R. Balda, V. Jubera, J.P. Chaminade, Fernàndez, J. Opt. Express 16 (2008) 2653.
[13] A.H. Reshak, A. Majchrowski, M. Swirkowicz, A. Klos, T. Lukasiewicz, I.V. Kityk, K. Iliopoulos, S. Couris, M.G. Brik, J. Alloys Compd. 481 (2009) 14.
[14] A.H. Reshak, S. Auluck, I.V. Kityk, A. Majchrowski, D. Kasprowicz, M. Drozdowski, J. Kisielewski, T. Lukasiewicz, E. Michalski, J. Mater. Sci. 41 (2006) 1927.
[15] Y. Li, Y. Wu, G. Zhang, P. Fu, X. Bai, J. Cryst. Growth 292 (2006) 468.
[16] P.E. Werner, L. Eriksson, M. Westdahl, J. Appl. Crystallogr. 18 (1985) 367.
[17] R.D. Shannon, Acta Crystallogr. A 32 (1976) 751.
[18] B.R. Judd, Phys. Rev. 127 (1962) 750.
[19] G.S. Ofelt, J. Chem. Phys. 37 (1962) 511.
[20] W.T. Carnall, P.R. Fields, K. Rajnak, J. Chem. Phys. 49 (1968) 4414.
[21] W.T. Carnall, P.R. Fields, K. Rajnak, J. Chem. Phys. 49 (1968) 4424.
[22] M.J. Weber, Phys. Rev. 157 (1967) 262.
[23] J.A. Caird, L.G. Deshazer, J. Nella, IEEE J. Quantum Electron. 11 (1975) 874.
[24] R. Reisfeld, The Rare Earths in Modern Sciences and Technology, Plenum Press, New York, 1979, pp. 2–441.
[25] M. Liu, B. Lu, H. Pan, Q. Song, Acta Opt. Sin. 8 (1988) 1079.
[26] L.D. Deloach, S.A. Payne, L.L. Chase, L.K. Smith, W.L. Kway, W.F. Krupke, IEEE J. Quantum Electron. 29 (1993) 1179.
[27] R. Guo, Y. Wu, P. Fu, F. Jing, Opt. Commun. 244 (2005) 321.
[28] P. Wang, J.M. Dawes, P. Decker, D.S. Knowles, J.A. Piper, B.S. Lu, J. Opt. Soc. Am. B 16 (1999) 63.
[29] H. Jiang, J. Wang, H. Zhang, X. Hu, B. Teng, P. Burns, J.A. Piper, Chem. Phys. Lett. 361 (2002) 499.
[30] F. Mougel, K. Dardenne, G. Aka, A. Kahn-Harari, D. Vivien, J. Opt. Soc. Am. B 16 (1999) 164.
[31] W.F. Krupke, IEEE J. Sel. Top. Quantum Electron. 6 (2000) 1287.